Normal shocks with high upstream pressure

William A. Sirignano*
Department of Mechanical and Aerospace Engineering, University of California, Irvine, California 92697, USA

(Received 20 March 2018; published 17 September 2018)

A normal compressive shock wave with supercritical upstream thermodynamic conditions is analyzed using the Soave-Redlich-Kwong equation of state (EoS) relations for real-gas density, enthalpy, and entropy for argon, nitrogen, oxygen, and carbon dioxide. Upstream pressure and temperature vary from 10 to 500 bar and 160 to 800 K. At high pressures, the flow does not follow the calorically perfect-gas behavior. For the perfect gas, the enthalpy and ratio of pressure-to-density are directly proportional to the square of the sound speed, allowing direct substitution of the sound speed in the conservation equations. A thermodynamic function is identified for the real-gas sound speed which is shown to remain as the proper characteristic speed. Although the sound speed does not emerge directly from the conservation equations as it does for a perfect gas, the shock speed goes to this limiting value as shock strength goes to zero. For the real gas, modifications are obtained for Prandtl's relation and the Rankine-Hugoniot relation. The modified real-gas Riemann invariants are constructed and discussed for application to weak shocks. A foundation is presented for use with other cubic EoS, multicomponent flows, and/or for more complex flow configurations. Near-similar solutions are developed by normalization of the variables using critical values for pressure and temperature. These exact solutions are compared with approximate solutions obtained via a linearization of the cubic EoS for deviation from ideal-gas behavior.

DOI: 10.1103/PhysRevFluids.3.093401

I. INTRODUCTION

The goal of this work is to analyze the differences at high pressures between real-gas compressible-flow behavior and ideal-gas compressible-flow behavior. Recent trends in liquid-propellant rocket engines and aircraft turbofan engines involve substantial increases in combustion-chamber pressures for the purpose of increased thermal efficiencies. In particular, critical pressures of the fluids are exceeded, and the ideal-gas assumption becomes flawed. Shock waves can appear in the compressor of a gas-turbine engine or in the propellant turbopumps of the rocket engines. If combustion instabilities develop in the engine combustor, shock waves become possible for higher amplitude oscillations. While these practical shocks might be oblique or curved, an analysis that begins with normal shocks is justified.

As a basis for analysis of compressible flow, two quantities which appear in the equations of motion (EoS) directly or implicitly must be related: enthalpy h and pressure-to-density ratio p/ρ. Also, their relations with temperature T and sound speed c are of interest. These four variables are related very simply for the ideal gas whereby h, p/ρ, c^2, and temperature T are all directly proportional to each other. In the following discussion, it is shown how much more complex the real gas can be due to the role of the attractive and repulsive forces between molecules at the high pressures and densities.

*sirignan@uci.edu

For analysis of compressible flow at very high pressures, corrections to the ideal-gas relations are needed in the supporting thermodynamics theory. Among other issues, many classical relations no longer apply in their original forms. In particular, adjustments are needed for the EoS that describe density (or specific volume), enthalpy (or internal energy), and sound speed as functions of pressure, temperature, and composition.

The potential for important quantitative differences for inviscid compressible flows between ideal-gas flows and real-gas flows has been well established in the literature. Zel'dovich and Raizer [1] give a broad coverage to the physics of shock waves and include several issues for real gases. Menikoff and Plohr [2] emphasize several mathematical features of the discontinuous solutions to the Riemann problem. There have been earlier attempts to determine the jump in flow variables across a shock wave. Tao [3] calculated jumps across normal shocks in Freon-12 flow. They assumed the Beattie-Bridgeman EoS and used perturbation theory with six small parameters to describe the thermodynamics. The results show significant variations from ideal-gas behavior for shocks with high pressure ratios. For a pressure ratio equal to 25, the downstream density was about 15% higher for the real gas compared to the ideal gas, while the real-gas downstream temperature was 25% lower. Shock flows of nitrogen were considered by Wilson and Regan [4] where the upstream pressure and temperature varied up to 1000 atmospheres and 2000 K. Correction factors as high as 1.6 for downstream pressure and 1.17 for downstream temperature were found to apply as multiples of the ideal-gas values. The analysis was based on the assumption that the upstream values satisfy the ideal gas law. For a wide range of upstream values of interest, this assumption is not acceptable. Koremenos and Antonopoulos [5] computed results for a normal shock in air using the Redlich-Kwong EoS. For a convergent-divergent nozzle with a standing shock in the divergent (supersonic) portion, both Arina [6] and Jassim and Muzychka [7] show significant (i.e., 10 % or more) differences in flow properties for the ideal gas and the real gas. The shock location is also modified. Similar magnitudes of differences are shown by Arina [6] for the shock tube problem with traveling shock, expansion wave, and contact surface. Recently Sirignano [8], using a linear approximation to the Soave-Redlich-Kwong (SRK) EoS, reported results for choked nozzle flow, nonlinear acoustics, and normal shocks for certain thermodynamic-parameter domains. All of these works reported only subsonic flow normal to the shock on the downstream side and supersonic flow upstream, the same as the classical findings of the ideal-gas behavior based on the Second Law constraint. The Bethe-Zel'dovich-Thompson fluid [9] is known to exhibit other types of strange behavior with shock waves and other flow issues. Those fluids are typically formed with very large molecules and are outside of the range of interest here.

Many different types of variations from ideal-gas flow behavior are described as real-gas phenomena in the general literature. Included are viscous flows, flows with heat and/or mass transport, and flows with various type of relaxation processes such as molecular vibrational excitations, dissociations, a wide variety of other chemical reactions, electronic excitations, and ionization. In this paper, those nonequilibrium processes are not addressed. Here the focus is on inviscid, compressible flows with equilibrium conditions that do not satisfy the ideal-gas law, $p = \rho RT$, and with enthalpy and internal energy dependent on pressure p as well as temperature T. For continuous flows, no nonequilibrium conditions are considered; for the normal shock wave, the thin zone of $O(100)$ nanometers in thickness with molecular translational and rotational nonequilibrium is treated as a mathematical discontinuity.

II. THERMODYNAMIC FOUNDATIONS

The formulation requires a replacement of the ideal-gas law with a relation that yields density ρ as a function of pressure p, temperature T, and composition in terms of species mole fractions X_i (or mass fractions Y_i). In addition, formulas are needed giving specific enthalpy h (or specific internal energy e), specific entropy s, and sound speed c as functions of those same variables. We need all of these relations to understand fully the state of the fluid.

TABLE I. Values for critical temperature, critical pressure, and ratio of specific heats, acentric factor, and S coefficient.

Gas	T_c (K)	p_c (kPa)	γ	W	ω	$S(\omega)$
Argon	150.8	4780	1.667	40.0	0	0.485
Nitrogen	126.2	3390	1.400	28.0	.040	0.547
Oxygen	154.6	5050	1.400	32.0	0.022	0.517
Carbon dioxide	304.25	7380	1.286	44.0	0.228	0.831
Water vapor	647.1	22064	1.333	18.0	0.344	1.001

A. EoS for density

The compressibility factor is defined as $Z \equiv p/(\rho RT)$. For the ideal gas, $Z = 1$ everywhere, while, for a real gas, it may vary with space and time. The cubic EoS gives molar specific volume v or mass density ρ for given pressure p and temperature T. In addition, an enthalpy departure function gives the difference between the enthalpy for the ideal gas and the enthalpy for the real gas at any given pressure and temperature. Essentially, there is a pair of EoS, one for density and another for enthalpy h. The developments proposed here may be done with any of the well-known cubic EoSs, but only one is chosen here. In particular, the analysis proceeds with the SRK cubic EoS [10], which is known for accuracy over a wide range of important applications. The SRK EoS is a modification of the van der Waals cubic EoS where some empirical fitting has been used to describe better the effects of molecular attraction and repulsion. Although only very simple configurations will be considered here (i.e., single species and single phase), an EoS is sought that can be extended reasonably well for use in more complicated configurations to allow consistency in future work.

The SRK EoS for a single-component fluid is

$$Z^3 - Z^2 + (A - B - B^2)Z - AB = 0, \tag{1}$$

where

$$\begin{aligned} Z &\equiv \frac{pv}{R_u T} = \frac{p}{\rho RT}, \quad A \equiv \frac{ap}{(R_u T)^2}, \quad B \equiv \frac{bp}{R_u T}, \\ a &\equiv 0.42748 \frac{(R_u T_c)^2}{p_c}\left[1 + S\left(1 - T_r^{0.5}\right)\right]^2, \quad b \equiv 0.08664 \frac{R_u T_c}{p_c}, \\ T_r &\equiv \frac{T}{T_c}, \quad S \equiv 0.48508 + 1.5517\omega - 0.15613\omega^2. \end{aligned} \tag{2}$$

R and R_u are the specific and universal gas constants, respectively. Subscript c denotes a thermodynamic critical value. The coefficients a and b (and therefore A and B) relate respectively to intermolecular attraction and repulsion.

An alternative form of Eq. (1) which is useful for certain algebraic manipulations is given as

$$Z - 1 = \frac{B}{Z - B} - \frac{A}{Z + B}. \tag{3}$$

When $A \ll 1$ and $B \ll 1$, Sirignano [8] has shown that a good approximation is given by $Z = 1 + B - A$.

For argon, oxygen and nitrogen, the difference in the ω value modifies S in the second significant digit; see Table I. (A different functional form is recommended for hydrogen; while discussion of gases with different formulas is omitted to avoid distraction from the main themes, the approach is easily extendable to consider them.) In the domain of pressure and temperature where both gas and liquid exist in equilibrium, there is a solution of Eq. (1) for each phase; thus, two different, physically meaningful Z values can result. Since p and T are identical for each phase, the implication is that there

are two values for the specific molar volumes v_g and v_l and thereby for the mass densities $\rho_g = W/v_g$ and $\rho_l = W/v_l$. W is the molar mass. A range of values is considered for p and T where only one phase exists and therefore only one interesting solution to the cubic equation exists. (Complex roots are ignored.) At supercritical conditions, there are ranges of p and T where a compressible fluid exists without discontinuities in properties and may still be labeled as a gas. Thus, reference to ρ and other properties are made with the understanding they apply to a gas.

Table I presents critical temperature T_c, critical pressure p_c, acentric factor ω, ratio of specific heats for the ideal gas γ, and molecular mass W for selected gases. Monatomic, diatomic, and triatomic species are considered. In the calculations in the following sections, argon, nitrogen, oxygen, and carbon dioxide are analyzed. γ, c_p, and c_v are values pertaining only to the ideal-gas EoS. For example, as shown by Eq. (6), c_p will not be the partial derivative of enthalpy with respect to temperature for the real gas. It will be that derivative only for the ideal gas, and it retains only that meaning when used in the real-gas enthalpy relation. This particular formulation allows each of the enthalpy and the entropy functions to be conveniently introduced as the ideal gas value plus a departure function.

There is no obvious way to collapse the behaviors of different gases to a similar form for ease of calculation. For example, even if pressure and temperature are normalized and p/p_c and T/T_c are treated, the gases differ significantly through three other parameters in the table: γ, ω, and W.

For a mixture of two or more gases, the parameters a and b are determined by the following rules. Each species in the mixture has its own value of the integer index i. Then the mixture values of a and b are determined from the species values a_i and b_i and the mole fractions X_i of the species as follows:

$$a \equiv \sum_{i=1}^{\tilde{N}} \sum_{j=1}^{\tilde{N}} X_i X_j (a_i a_j)^{0.5} (1 - k_{ij}); \quad b \equiv \sum_{i=1}^{\tilde{N}} X_i b_i \tag{4}$$

and

$$a_i \equiv 0.42748 \frac{(R_u T_{ci})^2}{p_{ci}} \alpha_i; \quad b_i \equiv 0.08664 \frac{R_u T_{ci}}{p_{ci}}; \quad \alpha_i \equiv \left[1 + S_i \left(1 - T_{ri}^{0.5}\right)\right]^2$$
$$T_{ri} \equiv \frac{T}{T_{ci}}; \quad S_i \equiv 0.48508 + 1.5517\omega_i - 0.15613\omega_i^2. \tag{5}$$

The extension to multicomponent gases will not be considered here. However, Eqs. (4) and (5) show that it would be straightforward.

B. Enthalpy and entropy departure functions

The specific enthalpy h (or enthalpy per mole $\tilde{h} = Wh$) deviates from the ideal-gas specific enthalpy h^* (or $\tilde{h}^*$) at the same temperature. For the SRK case, the enthalpy h satisfies the following relation:

$$h = \frac{\tilde{h}}{W} = h^*(T) + \frac{1}{W}\left[R_u T(Z-1) + \frac{T(da/dT) - a}{b} \ln \frac{Z+B}{Z}\right]. \tag{6}$$

Useful background information is given by Ref. [10]. It can be shown from Eq. (4) that, for a single species,

$$\tilde{a} \equiv 0.42748 \frac{(R_u T_c)^2}{p_c}, \quad T\frac{da}{dT} = \tilde{a}\left[S^2 \frac{T}{T_c} - S(S+1)\sqrt{\frac{T}{T_c}}\right], \quad T^2 \frac{d^2 a}{dT^2} = \frac{\tilde{a} S(S+1)}{2}\sqrt{\frac{T}{T_c}},$$
$$A \equiv \frac{ap}{(R_u T)^2} = \frac{\tilde{a} p}{(R_u T)^2}\left[(S+1)^2 - 2S(1+S)\sqrt{\frac{T}{T_c}} + S^2 \frac{T}{T_c}\right],$$

$$A' \equiv \frac{p}{(R_u T)^2} T \frac{da}{dT} = \frac{AT}{a}\frac{da}{dT} = \frac{\tilde{a}p}{(R_u T)^2}\left[S^2 \frac{T}{T_c} - S(S+1)\sqrt{\frac{T}{T_c}}\right],$$

$$A' - A = \frac{\tilde{a}p}{(R_u T)^2}(S+1)\left[S\sqrt{\frac{T}{T_c}} - (S+1)\right], \quad A'' \equiv \frac{AT^2}{a}\frac{d^2a}{dT^2} = \frac{\tilde{a}p}{(R_u T)^2}\frac{S(S+1)}{2}\sqrt{\frac{T}{T_c}}. \quad (7)$$

The enthalpy relation can be developed a little further using these definitions:

$$h(p,T) = h^*(T) + \frac{R_u T}{W}\left[Z - 1 + \frac{A' - A}{B}\ln\frac{Z+B}{Z}\right]$$

$$= c_p T + \left[(Z-1)RT + \frac{\tilde{a}}{bW}(S+1)\left[S\sqrt{\frac{T}{T_c}} - (S+1)\right]\ln\frac{Z+B}{Z}\right]. \quad (8)$$

Using the departure function, the entropy change between states 1 and 2 from the value for an ideal gas may be described [10] as follows:

$$\left.\frac{60}{01}S\right|_{\text{ideal}} = R\left(\frac{\gamma}{\gamma-1}\ln\frac{T_2}{T_1} - \ln\frac{p_2}{p_1}\right),$$

$$\frac{60}{01}S = \left.\frac{60}{01}S\right|_{\text{ideal}} + R\left(\ln\frac{Z_2 - B_2}{Z_1 - B_1} + \frac{A_1'}{B_1}\ln\frac{Z_1}{Z_1+B_1} - \frac{A_2'}{B_2}\ln\frac{Z_2}{Z_2+B_2}\right). \quad (9)$$

The speed of sound is evaluated for our specific EoS in Appendix A.

III. SHOCK RELATIONS

The conservation equations for mass, normal momentum, transverse momentum, and energy across the shock wave can be stated in the following forms:

$$\rho_1 u_1 = \rho_2 u_2 \equiv m, \quad (10)$$

$$\rho_1 u_1^2 + p_1 = \rho_2 u_2^2 + p_2, \quad (11)$$

$$w_1 = w_2, \quad (12)$$

$$h_1 + u_1^2/2 = h_2 + u_2^2/2, \quad (13)$$

where u and w are the normal and transverse velocity components, respectively. Subscripts 1 and 2 pertain respectively to conditions on the upstream and downstream sides of the shock. Upstream conditions for p_1, h_1, ρ_1, u_1, and w_1 are related to the downstream values p_2, h_2, ρ_2, u_2, and w_2. The other variables T_1 and T_2 can also be readily determined from the equations of state.

An examination indicates that $\sqrt{p/\rho}$ and $\sqrt{h}$ are the characteristic velocities appearing in the momentum equation (11) and energy equation (13), respectively. Fortunately, with the calorically perfect gas, those two values are directly proportional to each other and to the sound speed c over all upstream thermodynamic property values. Thus, sound speed is the characteristic velocity for the perfect gas. The ideal-gas shock strength (measured by the magnitude of the jump across the shock in the value of any thermodynamic property) decreases as shock velocity decreases towards the sonic speed and goes to zero as the sonic speed is reached. For the real gas, the values of $\sqrt{p/\rho}$, $\sqrt{h}$, c, and $\sqrt{T}$ will not be directly proportional to each other. Thus, a different behavior might be expected because no single characteristic velocity appears through the equations. So the question remains about whether the Mach number will be more informative than other nondimensional velocities. It is widely stated that the weak shock propagation velocity goes to the sound speed in the limit as its strength goes to zero. However, typically, the literature shows by theory that the limiting shock

velocity as $\delta p \to 0$ is the sound speed only after the perfect-gas EoS is assumed [11]. A proof that does not depend on the choice for the EoS is shown in Appendix B; the sound speed in the limiting speed for the real gas just as it is for the ideal gas. Thereby, it is the sensible choice for a reference velocity.

A. Solution method

The real-gas shock problem can be viewed as having ten flow properties: u, p, ρ, h, and T on both sides of the shock. The equations give seven constraints: three conservation equations [(10), (11), and (13)] applied across the shock and the thermodynamic relations (1) and (6) applied on each side of the shock. [The transverse velocity and transverse momentum equation (12) are dismissed here.] Thus, three conditions must be imposed. Upstream pressure p_1 and upstream temperature T_1 will be chosen to characterize a parameter case. Through the thermodynamic relations, the other upstream thermodynamic variables h_1, Z_1, and ρ_1 become known for that case. The downstream density ρ_2 value will then be chosen and varied over a range of interest, i.e., $\rho_2/\rho_1 \lesssim 1$. With the known densities, the velocity ratio u_2/u_1 is determined easily from the continuity equation (10), and u_2 can be eliminated from the two other conservation equations (11) and (13) by substitution. Then the momentum and energy equations can be combined to eliminate u_1 yielding

$$\frac{h_2 - h_1}{p_2 - p_1} = \frac{1}{2\rho_1}\left(1 + \frac{\rho_1}{\rho_2}\right) = \frac{\rho_2 + \rho_1}{2\rho_2\rho_1}, \tag{14}$$

where the right-hand side is now known. Equation (14) presents the classical Hugoniot relation. Substitution for h_2 in Eq. (14) using Eq. (6) gives a nonlinear two-equation system, together with Eq. (1), to determine p_2 and T_2. Numerical solution is needed and provided by the fsolve Matlab function: https://cn.mathworks.com/help/optim/ug/fsolve.html. After determining p_2 and T_2, Eq. (6) will yield h_2. Once all of these thermodynamic variables are known, the momentum and energy equations (11) and (13) will give u_1 and u_2 values pertaining to the chosen ρ_2 value. This completes the solution for all primitive variables. Nondimensional variables can be determined easily from these results.

Equations (10) and (11) can be combined to eliminate the velocities, thereby yielding the relation for the Rayleigh line:

$$p_2 - p_1 = m^2\left(\frac{1}{\rho_1} - \frac{1}{\rho_2}\right). \tag{15}$$

The intersection of the Hugoniot relation and Rayleigh line determines the thermodynamic conditions behind the shock. This is not surprising since those two statements result from the conservation equations that describe the jump conditions for the shock.

B. Rankine-Hugoniot relation

Let us examine same general features of the solution that are independent of the choice of EoS. Equation (14) can be rewritten using the following definitions: $\delta h \equiv h_2 - h_1$, $\delta\rho \equiv \rho_2 - \rho_1$, and $\delta p \equiv p_2 - p_1$. Also, $\rho^* \equiv (\rho_2 + \rho_1)/2$. Then Taylor expand each of ρ_1 and ρ_2 in the denominator about ρ^*. Also, expand h_2, h_1, p_2, and p_1 about the same point. If follows that $\delta h/\delta p = 1/\rho^* + O([\delta\rho]^2)$ where δp, δh, and $\delta\rho$ are of the same order. Thus, comparison with fundamental relation $Tds = dh - (1/\rho)dp$ demonstrates that entropy gain across the weak shock is $O([\delta p]^3)$ without regard to the particular EoS.

Equation (14) can be reformulated as

$$\frac{h_2}{h_1} = 1 + \frac{p_1}{2\rho_1 h_1}\left(1 + \frac{\rho_1}{\rho_2}\right)\left(\frac{p_2}{p_1} - 1\right). \tag{16}$$

In general, this cannot lead to a result where p_2/p_1 is simply a function of ρ_2/ρ_1 and γ such as we obtain for a perfect gas. That is, h_2/h_1 is not simply a function of p_2/p_1 and ρ_2/ρ_1 and $\rho_1 h_1/p_1$ is not a constant. So the generalization of the Rankine-Hugoniot curve does not give an impressive canonical form. This finding is consistent with the dependence on upstream conditions seen in Figs. 4(a), 4(b), and 10(a).

It is convenient to define and evaluate nondimensional ratios which take the value of one for the ideal gas but will vary with p and T for the real gas. Already, there is the compressibility factor $Z \equiv p/\rho RT$. The following ratios are added:

$$\mu \equiv \frac{(\gamma-1)\rho h}{\gamma p}; \quad \nu \equiv \frac{(\gamma-1)h}{c^2}; \quad \eta \equiv \frac{\gamma p}{\rho c^2}; \quad \nu \equiv \frac{c^2}{\gamma RT}. \tag{17}$$

Only three of these five ratios are independent, e.g., $\eta = \nu/\mu$, $\nu = Z\mu/$ Now $h_2/h_1 = (\mu_2/\mu_1)(p_2/p_1)/(\rho_2/\rho_1)$ which can be substituted in Eq. (16) to yield

$$\begin{aligned}
\frac{h_2}{h_1} &= \frac{\mu_2}{\mu_1}\frac{p_2}{p_1}\frac{\rho_1}{\rho_2} = 1 + \frac{\gamma-1}{2\gamma\mu_1}\left(1+\frac{\rho_1}{\rho_2}\right)\left(\frac{p_2}{p_1}-1\right), \\
\frac{\mu_2}{\mu_1} &= \frac{\frac{\rho_2}{\rho_1} + \frac{\gamma-1}{2\gamma\mu_1}\left(1+\frac{\rho_2}{\rho_1}\right)\left(\frac{p_2}{p_1}-1\right)}{\frac{p_2}{p_1}}.
\end{aligned} \tag{18}$$

For the ideal gas, with $\mu_1 = \mu_2 = 1$, p_2/p_1 becomes a function only of γ and ρ_2/ρ_1. However, for the real gas, it also depends on μ_2/μ_1 and μ_1. Thus, a different Rankine-Hugoniot curve results for different upstream conditions. Equation (18) indicates that the pressure ratio p_2/p_1 will become infinite when ρ_2/ρ_1 increases to a certain maximum value given by

$$\left.\frac{\rho_2}{\rho_1}\right|_{\max} = \frac{2\gamma\mu_2}{\gamma-1} - 1. \tag{19}$$

The implication is that μ_2 must reach an asymptote if ρ_2 reaches a maximum. Also when $\mu_2 = 1$ for the ideal gas, the maximum density ratio becomes $(\gamma+1)/(\gamma-1)$.

C. Modified Prandtl relation

We can define the velocity c^* and stagnation enthalpy h^o following normal practice:

$$h^o = h_1 + \frac{u_1^2}{2} = h_2 + \frac{u_2^2}{2} = \frac{\gamma+1}{2(\gamma-1)}c^{*2}. \tag{20}$$

From Eqs. (17), (B1), and (20), the following can be written as

$$\begin{aligned}
h_1 = \frac{\gamma\mu_1}{\gamma-1}\frac{p_1}{\rho_1} &= \frac{\gamma+1}{2(\gamma-1)}c^{*2} - \frac{u_1^2}{2}, \quad h_2 = \frac{\gamma\mu_2}{\gamma-1}\frac{p_2}{\rho_2} = \frac{\gamma+1}{2(\gamma-1)}c^{*2} - \frac{u_2^2}{2}, \\
u_1 - u_2 &= \frac{\gamma-1}{\gamma\mu_2 u_2}\left[\frac{\gamma+1}{2(\gamma-1)}c^{*2} - \frac{u_2^2}{2}\right] - \frac{\gamma-1}{\gamma\mu_1 u_1}\left[\frac{\gamma+1}{2(\gamma-1)}c^{*2} - \frac{u_1^2}{2}\right].
\end{aligned} \tag{21}$$

Convenient multiplication of the two major terms on the right by u_1/u_1 and u_2/u_2, respectively, allows the development of a new relation:

$$\frac{\gamma+1}{2\gamma}\frac{c^{*2}}{u_1 u_2} = \frac{(u_1-u_2)(\mu^{*2}-\delta^2)}{\mu_1 u_1 - \mu_2 u_2} + \frac{\gamma-1}{2\gamma}\frac{\mu_1 u_2 - \mu_2 u_1}{\mu_1 u_1 - \mu_2 u_2}, \tag{22}$$

where $\mu* \equiv (\mu_1+\mu_2)/2$ and $\delta \equiv (\mu_2-\mu_1)/2$. Equation (22) presents the modified-Prandtl shock relation. For the perfect gas where $\mu_1 = \mu_2 = 1$, the above relation becomes $c^{*2} = u_1 u_2$.

For the parameter range where $|\delta| \ll 1$, an approximation can be constructed, neglecting quantities of $O(\delta^2)$:

$$\frac{c^{*2}}{u_1 u_2} \approx 1 + \frac{2\gamma}{\gamma+1}\left[\mu^* - 1 + \frac{u_1+u_2}{u_1-u_2}\delta\right]. \tag{23}$$

Hence, the limiting velocity for the weak shock as $\mu* \to \mu_1$, $\delta \to 0$, and $u_2 \to u_1$ should be

$$S_L = u_1|_{\delta\to 0} = \frac{c^*}{\sqrt{1 + \frac{2\gamma}{\gamma+1}[\mu_1 - 1]}}. \tag{24}$$

Consequently, for the perfect gas, a relation results which is clearly consistent with previous findings [11]:

$$S_L = c^* = \sqrt{2(\gamma-1)h^o/(\gamma+1)} = \sqrt{2(\gamma-1)\left[c_1^2/(\gamma-1) + c_1^2/2\right]/(\gamma+1)} = c_1.$$

D. Nondimensional shock relations

It can be shown that normalization using critical values of pressure and temperature leads to a system of equations in nondimensional variables that has a greater degree of similarity across different gases. For example, it follows readily from Eqs. (1), (2), (4), and (5) that, for the same values of p/p_c, T/T_c, and ω, the same values of A, B, and Z result. Then the following normalization scheme can be employed:

$$\tilde{p} \equiv \frac{p}{p_c}; \quad \tilde{T} \equiv \frac{T}{T_c} = T_r; \quad \tilde{\rho} \equiv \frac{\rho R T_c}{p_c}; \quad \tilde{h} \equiv \frac{h}{RT_c}; \quad \tilde{s} \equiv \frac{s}{R};$$
$$\tilde{u} \equiv \frac{u}{\sqrt{RT_c}}; \quad \tilde{w} \equiv \frac{w}{\sqrt{RT_c}}; \quad \tilde{c} \equiv \frac{c}{\sqrt{RT_c}}; \quad M \equiv \frac{u}{c} = \frac{\tilde{u}}{\tilde{c}}. \tag{25}$$

Then Eqs. (10)–(13) can be rewritten as

$$\tilde{\rho}_1\tilde{u}_1 = \tilde{\rho}_2\tilde{u}_2, \tag{26}$$

$$\tilde{\rho}_1\tilde{u}_1^2 + \tilde{p}_1 = \tilde{\rho}_2\tilde{u}_2^2 + \tilde{p}_2, \tag{27}$$

$$\tilde{w}_1 = \tilde{w}_2, \tag{28}$$

$$\tilde{h}_1 + \tilde{u}_1^2/2 = \tilde{h}_2 + \tilde{u}_2^2/2, \tag{29}$$

where

$$\tilde{h}(\tilde{p},\tilde{T}) = \frac{\gamma}{\gamma-1}\tilde{T} + \left[(Z-1)\tilde{T} + 4.934(S+1)[S\sqrt{\tilde{T}} - (S+1)]\ln\frac{Z+B}{Z}\right],$$
$$\tilde{s}|_{\text{ideal}} = \left(\frac{\gamma}{\gamma-1}\ln\frac{\tilde{T}_2}{\tilde{T}_1} - \ln\frac{\tilde{p}_2}{\tilde{p}_1}\right),$$
$$\tilde{s} = \tilde{s}|_{\text{ideal}} + \left(\ln\frac{Z_2-B_2}{Z_1-B_1} + \frac{A_1'}{B_1}\ln\frac{Z_1}{Z_1+B_1} - \frac{A_2'}{B_2}\ln\frac{Z2}{Z_2+B_2}\right), \tag{30}$$
$$\tilde{c}^2 = Z\tilde{T}(f + g\beta). \tag{31}$$

The functions f and g depend only on $\tilde{p}$ and $\tilde{T}$ through A, B, and Z. β brings a dependence on $\gamma - 1$; see Eqs. (A6) and (A12). Consequently, specification of $\tilde{p}$, $\tilde{T}$, γ, and $S(\omega)$ determines $\tilde{h}$, $\tilde{s}$, and $\tilde{c}$. Since S is a weak function of ω, we can expect different gases at the same values of $\tilde{p}$, $\tilde{T}$, and

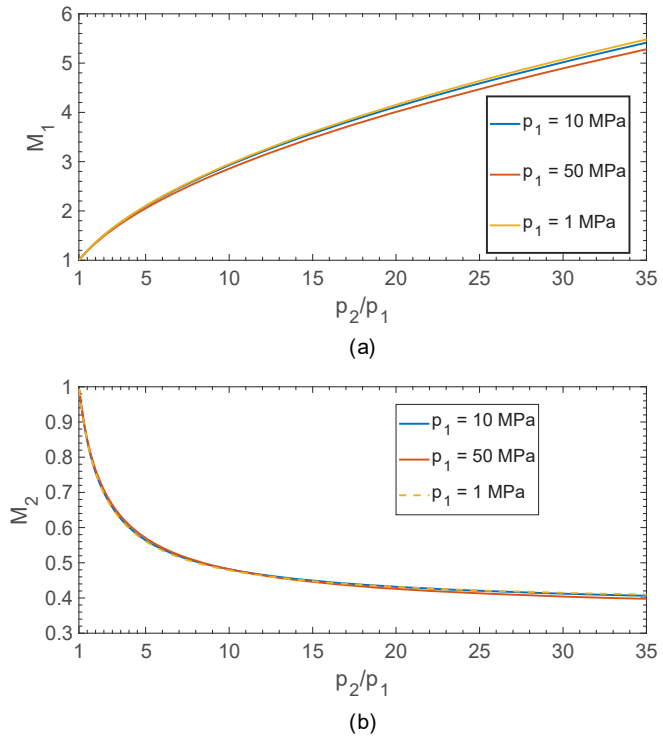

FIG. 1. Shock upstream and downstream Mach numbers for nitrogen at various upstream pressures $p_1 = 1$ MPA, 10 MPa, 50 MPa; and $T_1 = 400$ K. (a) M_1; (b) M_2.

γ to behave almost in a similar fashion. Also, the different behaviors for monatomic, diatomic, and triatomic gases at the same values of $\tilde{p}$ and $\tilde{T}$ primarily be due to differences in γ values.

E. Riemann invariants and weak shocks

Consider one-dimensional, unsteady wave motion with isentropic conditions. The continuity and momentum equations may be written in (x, t) space as

$$\frac{\partial(\ln\ \rho)}{\partial t} + u\frac{\partial(\ln\ \rho)}{\partial x} + \frac{\partial u}{\partial x} = 0, \quad \frac{\partial u}{\partial t} + u\frac{\partial u}{\partial x} + c^2\frac{\partial(\ln\ \rho)}{\partial x} = 0. \tag{32}$$

Define

$$\hat{c} \equiv \frac{\gamma - 1}{2}\int \frac{c}{\rho} d\rho \tag{33}$$

with the understanding that c and ρ are related along an isentrope in this integration. Multiplication of the continuity equation by c followed by sequential addition and subtraction with the momentum equation yields

$$\frac{\partial I_+}{\partial t} + (u + c)\frac{\partial I_+}{\partial x} = 0, \quad \frac{\partial I_-}{\partial t} + (u - c)\frac{\partial I_-}{\partial x} = 0, \tag{34}$$

where

$$I_+ \equiv u + \frac{2}{\gamma - 1}\hat{c}, \quad I_- \equiv u - \frac{2}{\gamma - 1}\hat{c}. \tag{35}$$

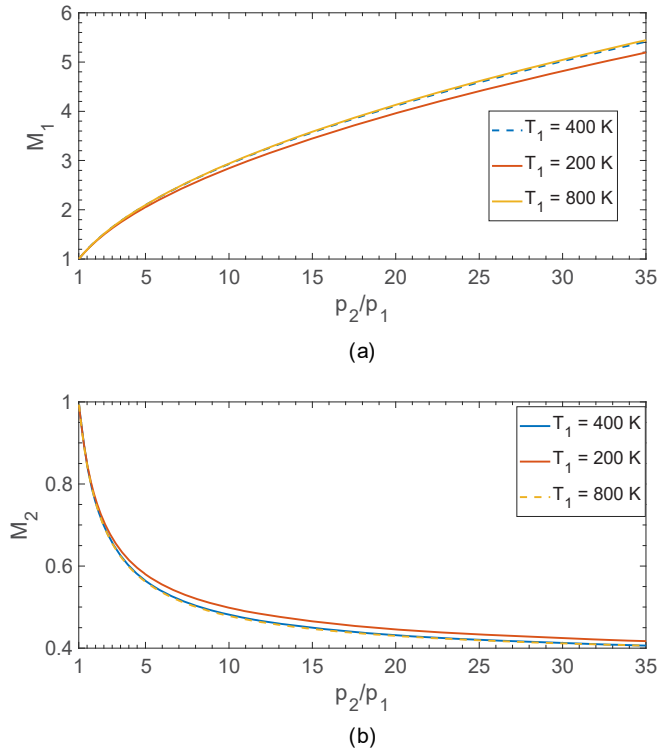

FIG. 2. Shock upstream and downstream Mach numbers for nitrogen at various upstream temperatures and $p_1 = 10$ MPa. (a) $T_1 = 200$ K; (b) $T_1 = 800$ K.

Thus, these modified Riemann invariants I_+ and I_- are constant along the paths $\delta x/\delta t = u + c$ and $\delta x/\delta t = u - c$, respectively. Lighthill [12] has discussed the integral of $1/(\rho c)$ over pressure and its role in invariancy. However, only results for a perfect gas were given. For the isentropic process, $(1/\rho c)dp = (c/\rho)d\rho$. For the perfect gas, integration readily shows that $\hat{c} = c$ for the indefinite integral (and $\hat{c} =$ [illegible] for the definite integral.).

For the real gas, the evaluation of $\hat{c}$ from the integral given by Eq. (33) requires coordination with the integrations of p, T, and Z along an isentropic path. From Eqs. (A11) and (A14), we have $dT = (\beta T/\rho)d\rho$ and $dp = c^2 d\rho$. Substitution can be made in Eq. (A2) to obtain $dZ = Z[c^2/p - (1+\beta)/\rho]d\rho$ along the isentropic path.

The evaluation of $\hat{c}$ can be thereby made through simultaneous solution of four coupled first-order ODEs between an initial and a final value of the independent variable, chosen here to be p:

$$\frac{d\hat{c}}{dp} = \frac{\gamma - 1}{2}\frac{1}{\rho c}, \quad \frac{d\rho}{dp} = \frac{1}{c^2}, \quad \frac{dZ}{dp} = Z\left[\frac{1}{p} - \frac{1+\beta}{\rho c^2}\right], \quad \frac{dT}{dp} = \frac{\beta T}{\rho c^2}. \tag{36}$$

Initial conditions are zero for $\hat{c}$ and the upstream values p_1, ρ_1, Z_1, and T_1 for the other properties. The solution values can be considered as running values of the end state for differing values of p_2/p_1.

If a weak shock were traveling in the positive x direction, the function I_- should remain constant across the shock through second order in the pressure jump since the entropy jump is third order. The velocity jump across the weak shock should approximately be

$$[\![u]\!] \approx \frac{2}{\gamma - 1}[\![\hat{c}]\!]. \tag{37}$$

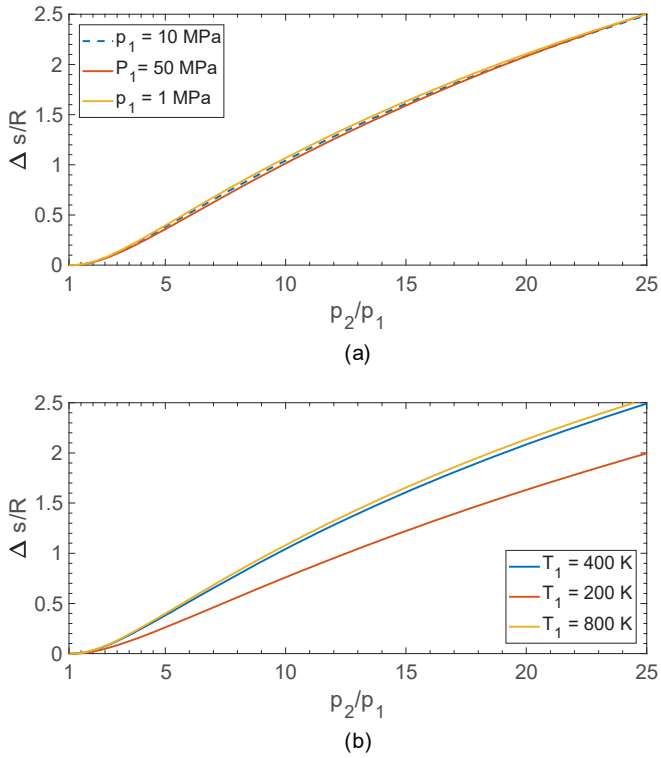

FIG. 3. Entropy vs shock Mach number for nitrogen at various upstream conditions. (a) $T_1 = 400$ K; $p_1 = 1$, 10, 50 MPa. (b) $p_1 = 10$ MPa; $T_1 = 200$, 400, 800 K.

The value of this velocity change is positive for a wave traveling in the positive x direction. Here the integral to evaluate $\hat{c}$ will have upper and lower limits set by downstream and upstream conditions, respectively. The shock relation (B1) gives exactly the magnitude of the velocity jump as $|\Delta u| = (p_2 - p_1)/(\rho_1 u_1)$. These two values for velocity jump can be compared for the same jump in pressure to test the weak shock assumption using Riemann invariants.

IV. RESULTS

A. Normalized velocities

From the examination of the conservation equations only, i.e., Eqs. (10), (11), and (13), three characteristic velocities appear explicitly: $\sqrt{p/\rho}$, $\sqrt{h}$, and $\sqrt{h^o}$. The last property is proportional to c^*, which will used in its place. For the perfect gas, $\sqrt{h}$, $\sqrt{p/\rho}$, and c are directly proportional to each other. So, the three normalized velocities, Mach number $M = u/c$, $u/\sqrt{\gamma p/(\rho)}$, and $u/\sqrt{(\gamma - 1)h}$ give identical values, and all take unity value as shock strength goes to zero. (The functions of γ are included in two of these normalizing velocities so that the speed of sound results in the limit of a perfect gas.) The fourth normalized velocity u/c^* generally has a different value from the others except at zero shock strength where again $u/c^* = 1$. One might get the sense that the sound speed is coincidentally important for the perfect gas but inconsequential for the real gas. However, the examination in the previous section shows that the relevance of the sound speed exists but is hidden in the thermodynamics. It is actually $\sqrt{p/\rho}$, $\sqrt{h}$, and c^* which lose consequence as characteristic velocities for the real gas while the importance of c remains. More discussion on these points is given in Sec. IV D.

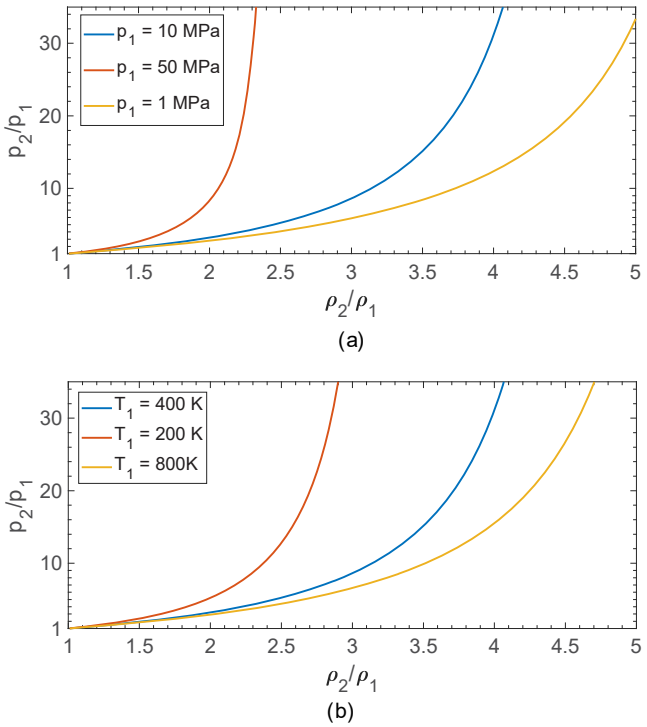

FIG. 4. Pressure ratio vs density ratio for nitrogen at various upstream conditions. (a) $T_1 = 400$ K; $p_1 = 1$, 10, 50 MPa. (b) $p_1 = 10$ MPa; $T_1 = 200$, 400, 800 K.

In the presentation of our computational results, the Mach number will be used as the normalized velocity.

B. Shock solutions

Various choices are made for upstream conditions in the ranges from 200 K $\leq T_1 \leq$ 800 K and 10 bar $\leq P_1 \leq$ 500 bar. All cases have supercritical temperature. One case has the 10-bar subcritical pressure with the value of a comparison with a "near-perfect" gas. Five different cases for upstream pressure and temperature are given in Figs. 1 through 4.

Figures 1 and 2 show how the upstream and downstream Mach numbers M_1 and M_2 vary with pressure ratio for nitrogen at various upstream conditions. The monotonic increase of M_1 with increasing pressure ratio is slightly less as upstream pressure increases and/or downstream temperature decreases. The monotonic decrease of M_2 is less affected with upstream pressure change but becomes slightly less as upstream temperature decreases. M_2 moves towards a constant asymptote as pressure ratio increases while M_1 continues to increase. The M_2 asymptote appears to be close to the ideal gas value of $\sqrt{(\gamma-1)/(2\gamma)}$.

Figure 3 shows that entropy goes to zero at the point where the shock strength goes to zero for all cases in Figs. 1 and 2. Although not shown, the calculated entropy jump would be negative at lower shock speeds where (prohibited) expansion shocks are predicted. The entropy gain is higher order in the jump value for pressure, velocity, or other variables; i.e., it decays more slowly to zero. At a given p_2/p_1 or M_1, the entropy gain is relatively insensitive to p_1 but increases as T_1 increases. At a fixed p_2/p_1 with increasing T_1, the value of M_1 increases modestly while c_1 increases faster; thereby, there is more kinetic energy $u_1^2/2$ to be dissipated, leading to the greater entropy gain.

Figure 4 shows pressure ratio versus density ratio for various upstream conditions. Unlike the perfect gas at a given value of γ, one curve does not apply to all upstream conditions for a given

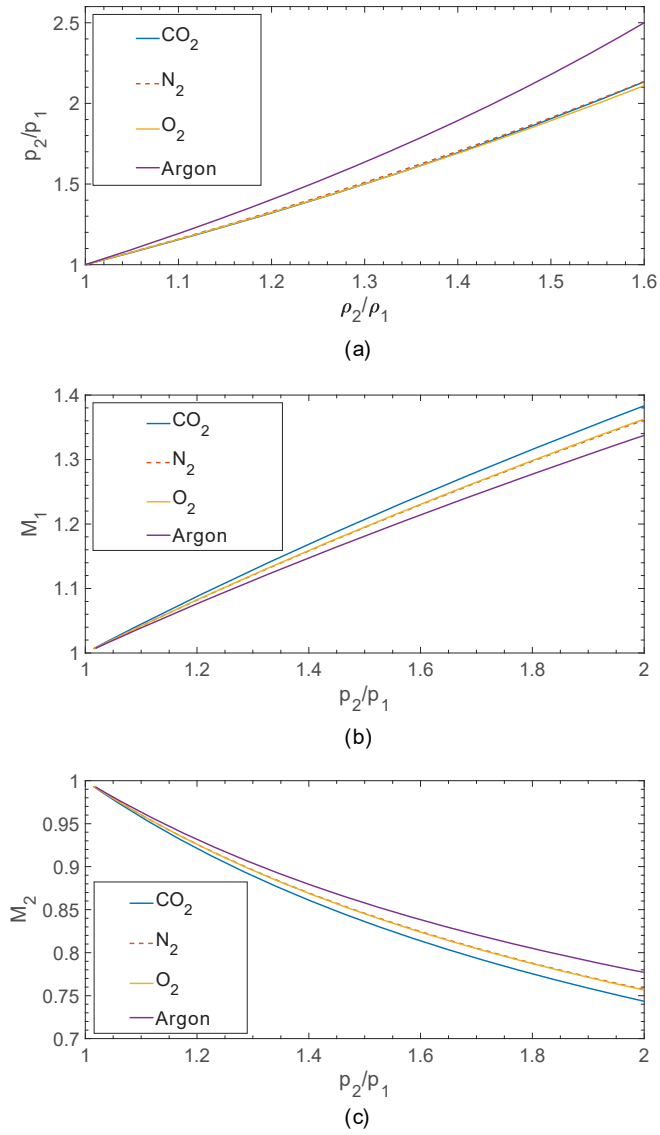

FIG. 5. Four-gas comparison at the same upstream conditions: $T_1 = 400$ K; $p_1 = 10$ MPa. (a) Pressure ratio vs density ratio; (b) M_1 vs pressure ratio; (c) M_2 vs pressure ratio.

gas. Strong dependence on both p_1 and T_1 is seen. The pressure ratio still goes towards infinity at a finite maximum value for density ratio. The maximum density ratio decreases with increasing p_1 and decreasing T_1. This limitation on maximum density is where the strongest departure from the ideal gas is seen.

The density ratio reaches a maximum value as predicted by Eq. (19). Essentially, the amount of compression of volume is limited no matter how high the pressure becomes. For the real gas, the parameter B affects this limit. B increases with p and decreases with T explaining how compression becomes more constrained at higher p_1 and lower T_1. The abscissa of Fig. 4 is equivalently u_1/u_2. So it is seen that velocities are very sensitive to upstream conditions.

The behaviors of four gases at identical upstream conditions are compared in Fig. 5: the two diatomic gasses, nitrogen and oxygen, the monatomic argon, and the triatomic carbon dioxide. Only

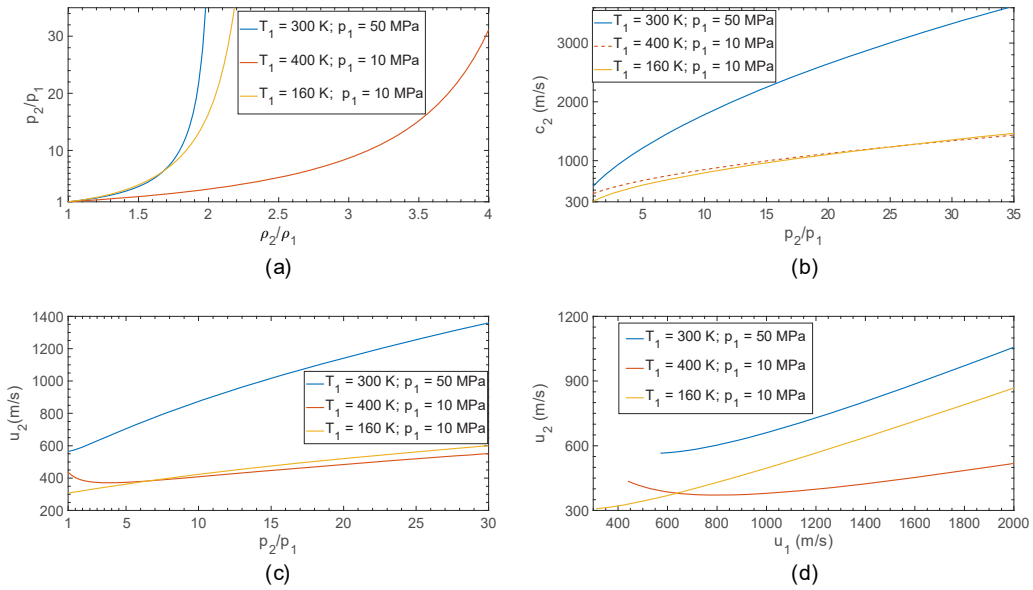

FIG. 6. Behavior of density ratio, downstream sound speed and velocity for nitrogen at various upstream conditions and pressure ratio: (a) Rankine-Hugoniot curves; (b) downstream sound speed vs pressure ratio; (c) downstream velocity vs pressure ratio; (d) downstream velocity vs upstream velocity.

the lower values of pressure ratio are considered; we expect strongly different behaviors closer to the values that produce maximum density ratio. The two diatomic gases have identical values of γ and values of the acentric factor ω [more importantly $S(\omega)$] and molecular mass W closer to each other than to the values for argon or carbon dioxide. The latter two gases have significant differences in their values for both γ and $S(\omega)$ but similar values for W. The three subfigures show that oxygen and nitrogen follow very similar behaviors, while the largest differences occur between the results for argon and carbon dioxide. We already know that γ is an important value for the ideal gas, and there is evidence here that it is true for the real gas as well. W does not appear to be a significant parameter in these plots since argon and carbon dioxide have different tracks in the plots. We are left with some uncertainty about the importance of ω.

For the applications of interest here, the behavior of the shock solutions with the SRK EoS is expected to satisfy the convexity condition which avoids unusual behavior such as wave splitting [2]. The convexity condition is given by the relation $\partial^2 p/\partial v^2|_s > 0$ for the downstream properties of the shock where $v = 1/\rho$. This condition is satisfied if both $\partial p/\partial\rho|_s = c^2 > 0$ and $\partial^2 p/\partial\rho^2|_s > 0$. The former condition is obviously satisfied by a positive value of c, and Fig. 5 gives a heuristic demonstration of the latter condition.

C. Behavior of downstream velocity

If density ratio reaches a limiting maximum value, the continuity equation with Eq. (19) assure that u_1/u_2 reaches a maximum value. In particular,

$$\left.\frac{u_1}{u_2}\right|_{\max} = \frac{2\gamma\mu_2}{\gamma - 1} - 1. \tag{38}$$

Consequently, as sufficiently high values of p_2/p_1 are reached, u_2 will monotonically increase with p_2/p_1. This trend occurs regardless of upstream conditions and applies also to the ideal gas.

Figure 6 compares downstream velocity behavior for three sets of upstream conditions. The behavior for $T_1 = 400$ K and $p_1 = 10$ MPa is most common and qualitatively similar to the ideal-gas

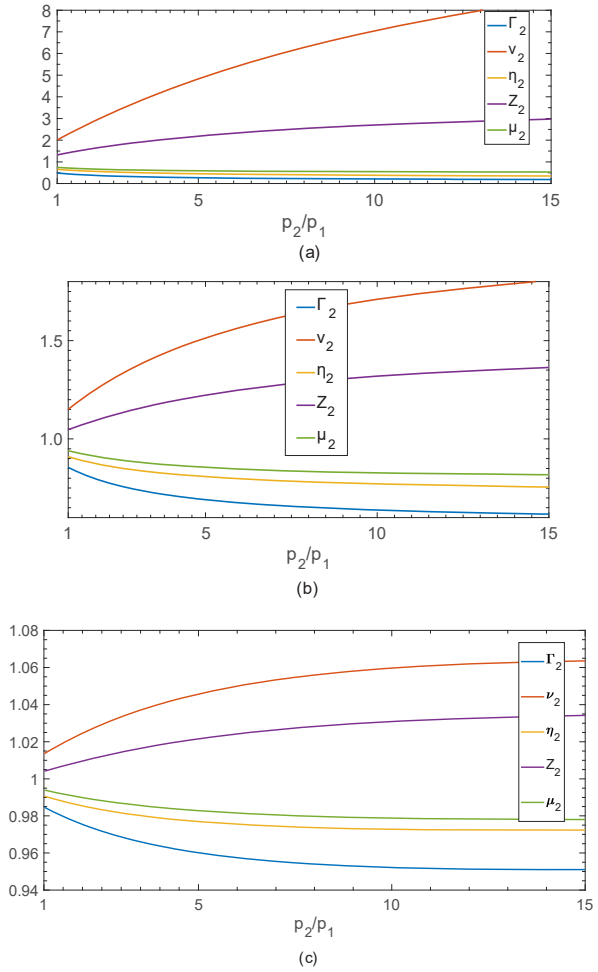

FIG. 7. Various ratios vs pressure ratio: variations from ideal-gas behavior for nitrogen at different upstream pressures. (a) 400 K, 50 MPa; (b) 400 K, 10 MPa; (c) 400 K, 1 MPa.

behavior. Namely, the limiting density ratio is not so small, say, greater than 5, and the downstream velocity decreases with increasing ratio until, at higher density ratio, it increases. For a substantial increase in p_1 or a substantial decrease in T_1, the behavior changes. In particular, the limiting density ratio is decreased by a significant factor and u_2 becomes monotonically increasing in u_1 or p_2/p_1 for the complete range. u_1 and c_2 are always monotonically increasing with p_2/p_1 for common gases. The linear asymptote for u_2 as a function of u_1 is a predictable consequence of the velocity ratio reaching a maximum constant value asymptotically as discussed before.

D. Departures from ideal-gas behavior

The five nondimensional ratios discussed early give useful information about where the departure from ideal-gas behavior is stronger. Figures 7–9 show Γ_2, ν_2, η_2, Z_2, and μ_2 versus pressure ratio. At $p_2/p_1 = 1$, the values apply to the upstream conditions. The departures from values of one indicate the variations from ideal gas behavior. Departures are seen to increase with increasing p_2/p_1 or equivalently with increasing M_1. They can become $O(1)$ at high pressures and/or low temperatures. At any upstream state, the departure magnitude increases with increasing p_2/p_1 or M_1, reaching an

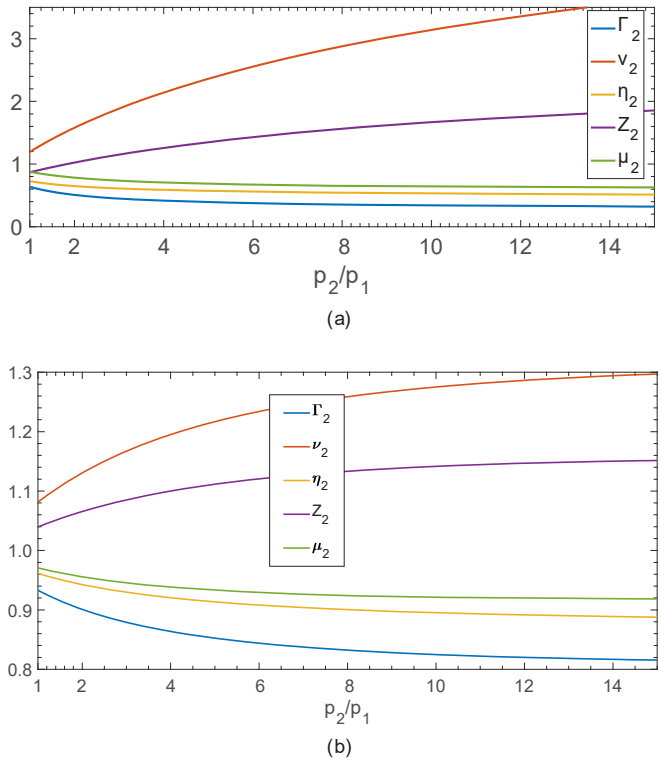

FIG. 8. Various ratios vs pressure ratio: variations from ideal-gas behavior for nitrogen at different upstream temperatures. (a) 200 K, 10 MPa; (b) 800 K, 10 MPa.

asymptote for some ratios. The greatest departures occur with and ν while the lowest departures occur with Z and μ.

There are certain implications from the behaviors seen. Since Z_2 and ρ_2 are reaching asymptotes, T_2 should asymptote linearly with p_2. $(\gamma - 1)h$ and $\gamma p/\rho$ are better aligned with each other than with c^2. So the modifications of Prandtl's relation and the Rankine-Hugoniot relation which both depend on μ values might not be as large as some other factors. The larger variation of c together with the small changes in M values implies that the variation in u must be very significant.

The case in Fig. 9 is interesting because it likely will apply to flow around compressor blades in the high-pressure gas-turbine engines of the not-so-distant future. It demonstrates that departures from ideal-gas behavior can be significant there.

E. Near-similar behavior

A comparison among argon, oxygen, nitrogen, and carbon dioxide is made holding the ratios p_1/p_c and T_1/T_c fixed at 8.00 and 2.00, respectively. γ is identical for both oxygen and nitrogen. Except for the slight (6%) difference in the values of $S(\omega)$, mathematical similitude of the nondimensional variables could be claimed for oxygen and nitrogen. Of course, only near-similitude can be expected. Argon and carbon dioxide differ in the values of both γ and $S(\omega)$ from each other, oxygen, and nitrogen by larger percentages. Figure 10(a) shows that the Rankine-Hugoniot curves (pressure ratio versus density ratio) are almost identical for oxygen and nitrogen. The RH curves are notably different for argon and carbon dioxide, indicating the important role of γ here. The curves for oxygen and nitrogen are extremely close, while the argon and carbon dioxide curves show respectively a larger and smaller pressure ratio for the same density ratio. Downstream Mach number as a function of

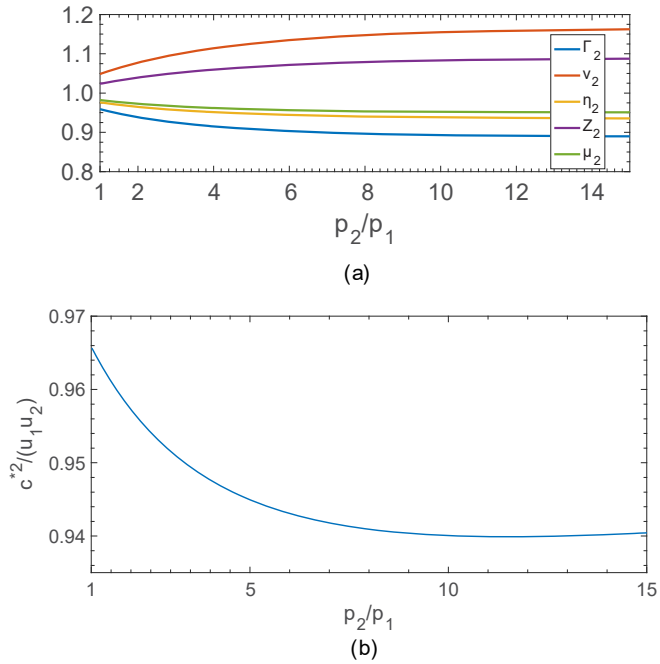

FIG. 9. Variations from ideal-gas behavior for nitrogen at upstream conditions of 800 K, 6 MPa. (a) Various ratios vs pressure ratio showing departures from unity values; (b) $c^{*2}/(u_1u_2)$ where departure from unity value is a real-gas affect.

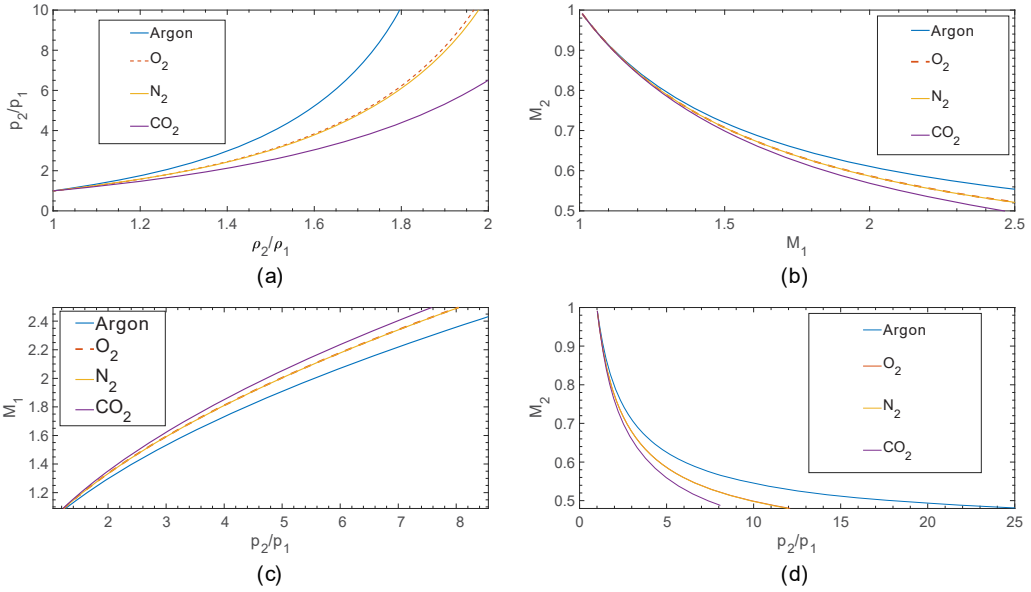

FIG. 10. Comparison of nitrogen, oxygen, and carbon dioxide for $p_1/p_c = 8.00$, $T_1/T_c = 2.00$. (a) Pressure ratio vs density ratio. (b) Downstream Mach number vs upstream Mach number. (c) Upstream Mach number versus pressure ratio. (d) Downstream Mach number versus pressure ratio.

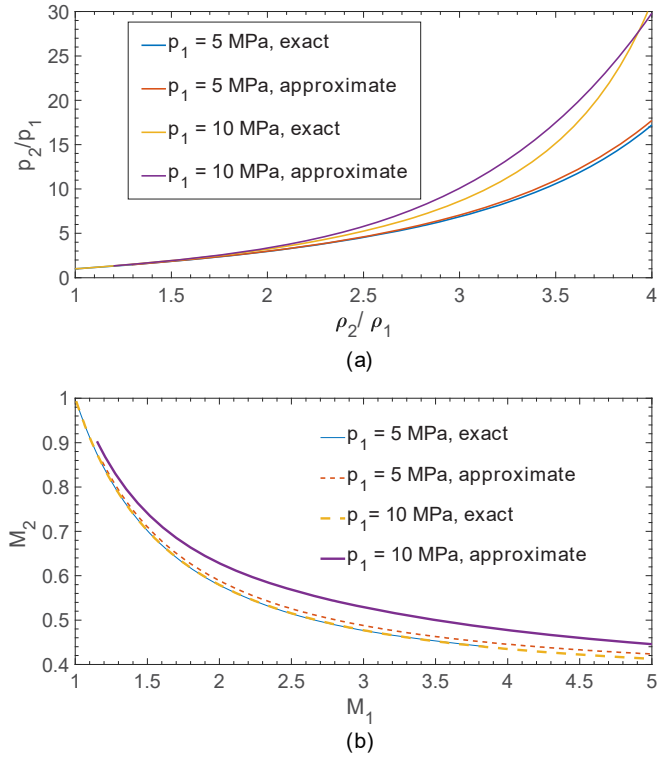

FIG. 11. Comparison of exact and approximate methods for nitrogen: $p_1 = 5$ MPa, 10 MPa; $T_1 = 400$ K. (a) Pressure ratio vs density ratio. (b) Downstream Mach number vs upstream Mach number.

upstream Mach number is presented in Fig. 10(b). Figures 10(c) and 10(d) show that for the same upstream or downstream Mach number, the monatomic (triatomic) species yields a larger (smaller) pressure ratio than the diatomic species. This limited study indicates that the critical values of pressure and temperature and γ are more important than the acentric factor ω in determining shock solutions.

F. Comparison with other real-gas normal shock calculations and experiment

Solutions for normal shocks for an SRK gas were first analyzed in Ref. [8] using a linear approximation of the cubic EoS. The nonlinearities of the flow conservation equations were fully preserved, but the solution of the cubic equation was given by $Z = 1 + B - A$, which is a valid linear approximation when $A \ll 1$ and $B \ll 1$. Here we compare results for our exact results with the approximate results for nitrogen with $p_1 = 5$ and 10 MPa and $T_1 = 400$ K. In Fig. 11(a) the Rankine-Hugoniot curves are shown. Again, for higher upstream pressures, a higher pressure ratio is obtained for the same value of density ratio with both the exact and the approximate solutions. For an upstream value of $p_1 = 5$ MPa, the error in the approximation is small. However, the error for $p_1 = 10$ MPa is more substantial because the values of A and B become larger. Fig. 11(b) shows downstream Mach number M_2 versus upstream Mach number M_1. Again, the error with the approximate solution is modest for $p_1 = 5$ MPa but becomes significant at 10 MPa. As expected from previous calculations, the M_2 versus M_1 curve for the exact solution is insensitive to p_1; however, the approximate solution shows more sensitivity, indicating an error. Of course, the ideal gas curves for both subfigures would not vary with upstream pressure or temperature for a fixed gas.

Table II compares the present nitrogen results, now designated by subscript S, with the results for air of Kouremenos and Antonopoulos [5], now designated by subscript KA. Ratios of pressure

TABLE II. Comparison with Kouremenos and Antonopoulos [5] normal shock calculations. Values for upstream Mach number, downstream Mach number, temperature ratio, and pressure ratio. Upstream values were 700 K and 4 MPa.

M_1	M_{2KA}	M_{2S}	$(T_1/T_2)_{KA}$	$(T_1/T_2)_S$	$(p_1/p_2)_{KA}$	$(p_1/p_2)_S$
1.5	0.70	0.700	0.77	0.757	0.40	0.404
2.0	0.58	0.577	0.60	0.593	0.23	0.221
2.5	0.52	0.514	0.49	0.470	0.15	0.140
3.0	0.47	0.476	0.39	0.375	0.10	0.0966
3.5	0.45	0.452	0.31	0.303	0.07	0.0706
4.0	0.44	0.435	0.26	0.248	0.06	0.0557

and temperature plus downstream Mach number are compared for certain upstream Mach numbers. The *KA* computations were done for a normal shock using the Redlich-Kwong EoS while the *S* results treat a normal shock using the SRK EoS. The quantitative KA results were interpreted from the graph in Fig. 2 of their paper; so the number of trusted significant digits is limited. Table II shows that the two results compare favorably. For the chosen range of M_1, Z_2 varied from 1.02 to 1.06 in the *S* results, increasing with M_1; and the downstream pressure, temperature, and density were each lower than the value yielded for the ideal gas, with the difference increasing with M_1.

Experimental evidence for shock waves at very high pressures is limited. Some comparison can be made with the experimental results of Dattelbaum *et al.* [13] for a shock in argon generated by gas-gun-driven plate impact. A comparison can be made at conditions below which they find that ionization becomes a factor and the downstream density exceeds the theoretical asymptote for nonionized conditions. First, the results at the highest upstream density value of $\rho_1 = 56.3$ kg/m^3 were considered with $T_1 = 293.8$ K. The calculation shows an asymptote for $\rho_2/\rho_1 = 3.489$ as shock velocity is increased. This is notably below the ideal-gas asymptotic ratio equal to 4.000 which applies for any upstream values. In the calculations here, density ratio is an input; so only the lowest value of shock velocity at the asymptote was yielded, which is $u_1 = 1945$ m/s. The experiment of Dattelbaum *et al.* does not reach velocities as low as this value; see their Fig. 2(b). For this upstream density value, they show only results where ionization was a factor and higher density ratios were obtained. The calculated results here does agree well with the fit they show using their Sesame 5172 database for the EoS. Next, the results at their lowest upstream density value of $\rho_1 = 24.9$ kg/m^3 are considered with $T_1 = 295.8$ K. Here the calculated asymptote is $\rho_2/\rho_1 = 3.70$ with the shock speed $u_1 = 2290$ m/s which agrees well with the results in Fig. 2(b) of Dattelbaum *et al.*

G. Comparison with weak shock approximation

From solutions to Eqs. (36) and (37) and the relation $Z = p/(\rho RT)$, the approximations to density ratio, pressure ratio, and velocity jump across the normal shock may be determined. In Fig. 12(a) the velocity jump $u_1 - u_2$ is calculated for a real gas over a range of shock strengths as described by pressure ratio. Nitrogen at upstream condition 10 MPa and 400 K is considered. Three methods are compared: the exact solution outlined in Sec. III A, the approximate method described in Sec. III E using the Riemann invariant developed for the real gas, and the inappropriate approximation which uses the Riemann invariant in a form developed only for the ideal gas with $\hat{c}$ replaced by $c_2 - c_1$. Figure 12(b) shows the Rankine-Hugoniot curve with comparison between the exact solution of Sec. III B and the approximate method of Sec. III E.

The use of the classical form of the Riemann invariant for weak shock estimation is seen to lead to great error because $\hat{c}$ is substantially smaller than $c_2 - c_1$. The modified Riemann invariant allows for a very good approximation with a pressure ratio below 1.5 and errors of only a few percent at $p_2/p_1 = 2.0$. The isentropic approximation based on the modified Riemann invariant underestimates the magnitude of the velocity difference and overestimates the density ratio for a

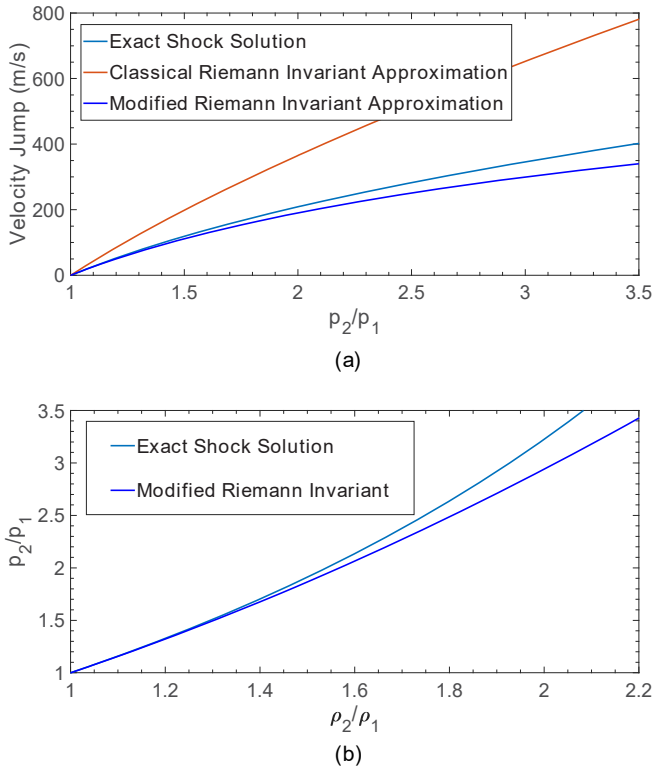

FIG. 12. Comparisons between exact shock solution and weak-shock approximation for nitrogen at upstream conditions of 400 K, 10 MPa. (a) Velocity jump vs pressure ratio; (b) Rankine-Hugoniot curve.

given value of the velocity ratio. Through the continuity equation, this can readily be shown to imply that both u_2 and u_1 are underestimated. This finding is consistent with expectations based on thermodynamic constraints. For a given pressure increase, the nonisentropic process requires a larger enthalpy increase. The change in enthalpy across the shock equals the change in kinetic energy per unit mass; thus, the nonisentropic process yields the larger velocity change.

V. CONCLUDING REMARKS

The Soave-Redlich-Kwong (SRK) EoS relations for real-gas density, enthalpy, and entropy relations for argon, nitrogen, oxygen, and carbon dioxide are used to analyze normal compressive shock waves under supercritical upstream thermodynamic conditions. Upstream pressure and temperature vary from 10 to 500 bar and 160 to 800 K. At high pressures, the flow does not follow the calorically perfect-gas behavior.

The $\sqrt{p/\rho}$ and $\sqrt{h}$ are characteristic velocities that appear in the primitive form of the conservation equations. For the perfect gas, those quantities are directly proportional to the sound speed, allowing direct substitution of the sound speed in the conservation equations. This cannot happen for the real gas. A new thermodynamic function is identified for the real-gas sound speed. Although the sound speed does not emerge directly from the conservation equations as it does for a perfect gas, the shock speed is shown to go to this limiting value as shock strength goes to zero. Thus, the sound speed remains as the proper characteristic speed. The deviation of the sound speed c from the values of $\sqrt{\gamma p/\rho}$, $\sqrt{(\gamma-1)h}$, or $\sqrt{\gamma RT}$ can be very substantial at higher pressures.

For the real gas, modifications are obtained for Prandtl's relation and the Rankine-Hugoniot relation. The upstream and downstream shock velocities, u_1 and u_2, for the real gas do not go to $c*$ as shock strength goes to zero (i.e., $p_2/p_1 \to 1$). The maximum density ratio $\rho_2/\rho_1|_{max}$ decreases and the minimum velocity ratio $u_2/u_1|_{min}$ increases as upstream pressure increases or upstream temperature decreases. Thereby, the largest deviations from a normal shock in an ideal gas at the same pressure ratio appear in the downstream density, the shock velocity, and the downstream velocity. Differences in upstream and downstream Mach numbers are smaller.

The SRK real gas has the parameters for the critical values p_c, T_c, and the accentric factor ω in addition to the specific-heat ratio γ and molecular mass W which also appear for the perfect gas. Near-similar solutions are developed by normalization of the variables using critical values for pressure and temperature. For the normalized solutions, γ has a significant effect as it does for the perfect gas. However, nitrogen and oxygen give near similar behaviors, indicating that ω and W carry less importance. Argon and carbon dioxide have molecular masses within 10% of each other (a lower fractional difference than oxygen and nitrogen) but a substantial difference in γ, leading to significant differences.

These exact solutions are compared with approximate solutions obtained via a linearization of the cubic EoS [8] for deviation from ideal-gas behavior. That approximation is built on the constraint that the compressibility factor Z satisfies $Z - 1 \ll 1$. The approximation with nitrogen is shown to perform well at 5 MPa but not so well at 10 MPa.

The results here for nitrogen are shown to agree well with results in Ref. [5], which used the Redlich-Kwong EoS for air.

Holding one Riemann invariant constant through a weak shock, a comparison is made with the weak shock approximation. A new real-gas Riemann invariant must be constructed. The new function $\hat{c} \equiv [(\gamma - 1)/2] \int (c/\rho) d\rho$ replaces the sound speed c in the modified Riemann invariant. At pressure ratios below 1.5, a good approximation is given by the approximate isentropic solution with the constant Riemann invariant.

A foundation is presented for use with other cubic equations of state, multicomponent flows, and/or for more complex flow configurations.

ACKNOWLEDGMENTS

This research was supported by the Air Force Office of Scientific Research under Grant FA9550-15-1-0033.

APPENDIX A: SOUND SPEED

The speed of sound can be evaluated for our specific EoS. The differential form of Eq. (1) is obtained as

$$[3Z^2 - 2Z + A - B - B^2]dZ + [Z - B]dA - [Z + 2BZ + A]dB = 0. \tag{A1}$$

Changes in A and B are forced by changes in T and p for constant-composition situations. These in turn cause changes in Z. It follows from the EoS that

$$dZ = Z\left[\frac{dp}{p} + \frac{dv}{v} - \frac{dT}{T}\right] = Z\left[\frac{dp}{p} - \frac{d\rho}{\rho} - \frac{dT}{T}\right], \tag{A2}$$

$$dA = A\left[\frac{dp}{p} - 2\frac{dT}{T}\right] + A'\frac{dT}{T}, \tag{A3}$$

$$dB = B\left[\frac{dp}{p} - \frac{dT}{T}\right], \tag{A4}$$

where $A' \equiv (T/a)(da/dT)A$.

Equations (A1) and (A2)–(A4) may be combined to determine the differential of pressure dp as a function of the temperature and density differentials, dT and $d\rho$. Specifically,

$$\frac{dp}{p} = f(A, B, Z)\frac{d\rho}{\rho} + g(B, Z)\frac{dT}{T}, \tag{A5}$$

where the definitions are made that

$$f(A, B, Z) \equiv \frac{2Z^3 - Z^2 + AB}{Z^3 - B^2 Z}, \quad g(B, Z) \equiv \frac{1}{Z - B} - \frac{A'}{Z(Z + B)}. \tag{A6}$$

From Eq. (6), the differential relation for enthalpy is derived:

$$dh = c_{\mathrm{p}} dT + \frac{R_{\mathrm{u}} T}{W}\left[(Z - 1)\frac{dT}{T} + dZ - \frac{A - A'}{B}\left(\frac{1}{Z + B} - \frac{1}{Z}\right)dZ - \frac{A - A'}{B}\frac{1}{Z + B}dB + \left(\frac{A''}{B}\ln\frac{Z + B}{Z}\right)\frac{dT}{T}\right]. \tag{A7}$$

From Eq. (9), the differential entropy becomes

$$\frac{ds|_{\mathrm{ideal}}}{R} = \frac{\gamma}{\gamma - 1}\frac{dT}{T} - \frac{dp}{p},$$
$$\frac{ds}{R} = \frac{ds|_{\mathrm{ideal}}}{R} + \frac{dZ - dB}{Z - B} + \frac{A'}{B}\left(\frac{1}{Z + B} - \frac{1}{Z}\right)dZ + \frac{A'}{B}\frac{1}{Z + B}dB + \left(\frac{A''}{B}\ln\frac{Z + B}{Z}\right)\frac{dT}{T}. \tag{A8}$$

As a check on the real-gas analysis here, another relation given by the combined First and Second Law is used:

$$\frac{dp}{\rho} = dh - T ds. \tag{A9}$$

Substitution for dh and ds from Eqs. (A7) and (A8) and use of (A2)–(A4), after substantial cancelations and simplification using (3), yields

$$\frac{dh - T ds}{RT} - \frac{dp}{\rho RT} = -\left[Z + \frac{A}{Z + B} + \frac{Z}{Z - B}\right]\frac{d\rho}{\rho} = 0. \tag{A10}$$

Thus, the consistency with fundamental thermodynamics is demonstrated which will become important later in determining the limiting speed of a shock as its strength (e.g., pressure jump) goes to zero.

With use of the differential forms given by Eqs. (A2)–(A4) for substitution into Eq. (A8), it follows that

$$\frac{dT}{T} = \beta\frac{d\rho}{\rho} + \frac{1}{c_v + \kappa}ds, \tag{A11}$$

where the following definitions are used:

$$\beta \equiv \frac{(\gamma - 1)Zg}{1 + \kappa/c_{\mathrm{v}}}, \quad \kappa \equiv c_{\mathrm{v}}(\gamma - 1)\frac{A''}{B}\ln\left(\frac{Z + B}{Z}\right). \tag{A12}$$

Eliminate the temperature differential by substitution from Eq. (A5) with Eq. (A11):

$$\frac{dp}{p} = (f + g\beta)\frac{d\rho}{\rho} + \frac{1}{c_{\mathrm{v}} + \kappa}ds. \tag{A13}$$

Thus, this results shows by using the chain rule that

$$c^2 \equiv \left.\frac{\partial p}{\partial \rho}\right|_s = \frac{Z R_u T}{W}(f + g\beta). \tag{A14}$$

The development of the wave equation for an inviscid fluid (in either linear or nonlinear form) shows that $c = \sqrt{\partial p/\partial \rho|_s}$ is the wave speed, commonly named the sound speed. For an ideal gas, $Z = 1$, $A = B = A' = A'' = 0$, $f = g = 1$, $\alpha = 0$, $\beta = \gamma - 1$ and therefore the well known result, $c^2 = \gamma R_u T/W$, follows.

APPENDIX B: CHARACTERISTIC VELOCITY

The continuity and momentum equations (10) and (11) can be combined to yield

$$p_2 - p_1 = \rho_1 u_1 (u_1 - u_2) = u_1^2 \frac{\rho_1}{\rho_2}(\rho_2 - \rho_1), \tag{B1}$$

thereby

$$\frac{\Delta p}{\Delta \rho} = u_1^2 + O(\Delta p). \tag{B2}$$

This implies that the limiting shock speed, identified here as S_L, as $\Delta p \to 0$ is given by the limiting value of u_1; that is,

$$S_L \equiv u_1|_{\Delta p, \Delta \rho \to 0} = \sqrt{\left.\frac{\Delta p}{\Delta \rho}\right|_{\Delta p, \Delta \rho \to 0}}. \tag{B3}$$

The proper characteristic speed that gives the limiting velocity of a weak shock wave can be obtained by examining the limiting behavior of the constraints of Eqs. (14) and (B1), which were developed from the conservation equations without regard to any particular EoS.

It follows from Eqs. (6) and (9) that, after certain cancelations and neglect of other higher-order terms:

$$\frac{\Delta h - T_1 \Delta s}{R T_1} = -\frac{\Delta T}{T_1} + \frac{\Delta p}{p_1} - \frac{\Delta Z - \Delta B}{Z_1 - B_1} - \frac{A_1}{B_1}\left(\frac{\Delta Z + \Delta B}{Z_1 + B_1} - \frac{\Delta Z}{Z_1}\right). \tag{B4}$$

Equation (3) can be used to substitute for $A_1/(Z_1 + B_1)$ in the last term of Eq. (B4). Also, Eqs. (A1)–(A4) are used to relate $\Delta T/T_1$, $\Delta Z/Z_1$, $\Delta A/A_1$, and $\Delta B/B_1$ to $\Delta p/p_1$ and $\Delta \rho/\rho_1$. The result is

$$\begin{aligned}\frac{\Delta h - T_1 \Delta s - \frac{\Delta p}{\rho_1}}{R T_1} &= \frac{\Delta h}{R T_1} - Z_1 \frac{\Delta p}{p_1} \\ &= \frac{f_1}{(\gamma - 1) g_1}\left[1 + \frac{\kappa_1}{c_v} + (\gamma - 1) g_1^2 Z_1\right]\frac{\Delta \rho}{\rho_1} - \frac{1}{(\gamma - 1) g_1}\left[1 + \frac{\kappa_1}{c_v}\right]\frac{\Delta p}{p_1},\end{aligned} \tag{B5}$$

where f, g, and κ are defined in Eqs. (A6) and (A12). Note that, since Δs is actually of higher order, Eq. (B5) is giving the limiting behavior of Eq. (14). Thus, the following limiting behavior for the propagation speed is actually influenced by each of the energy, momentum, and continuity constraints.

The left side of Eq. (B5) is known from Eq. (14) to become zero in the limit as $\Delta p \to 0$. So the right side must yield zero in that limit as well, which gives the relation

$$\left.\frac{\Delta p}{\Delta \rho}\right|_{\Delta p, \Delta \rho \to 0} = \left\{\frac{p}{\rho}\left[f + \frac{(\gamma - 1) g^2 Z}{1 + \kappa/c_v}\right]\right\}, \tag{B6}$$

where the definition of the thermodynamic function S_L providing the limiting shock speed S_L is obtained by matching the results from Eqs. (B3) and (B6):

$$S_L \equiv \left\{ \frac{p}{\rho} \left[f + \frac{(\gamma - 1) g^2 Z}{1 + \kappa / c_v} \right] \right\}^{0.5} . \tag{B7}$$

Compare this result with the relation given by Eq. (A14). This limiting shock speed is precisely the sound speed based on the upstream pressure and temperature. The perfect gas has $f = g = Z = 1$ and $A' = B = \kappa = 0$ yielding $S_L = (\gamma p/\rho)^{0.5} = c$, the sound speed.

Lighthill [12], following Hugoniot, gives a parallel argument using internal energy and specific volume instead of the enthalpy and density used here. He also shows graphically how entropy gain is related to the pathway between upstream and downstream conditions.

[1] Ya. B. Zel'dovich and Yu. P. Raizer, *Physics of Shock waves and High-Temperature Hydrodynamic Phenomena*, edited by W. D. Hayes and R. F. Probstein (Dover, Mineola, NY, 2002).

[2] R. Menikoff and B. J. Plohr, The Riemann problem for fluid flow of real materials, Rev. Mod. Phys. **61**, 75 (1989).

[3] L. N. Tao, Gas dynamic behavior of real gases, J. Aeronaut. Sci. **22**, 763 (1955).

[4] J. L. Wilson and J. D. Regan, A simple method for real gas flow calculations, Current Paper 772, UK Ministry of Aviation, Aeronautical Research Council, S. O. Code Number 23-9015-72 (1965), http://naca.central.cranfield.ac.uk/reports/arc/cp/0772.pdf.

[5] D. A. Kouremenos and K. A. Antonopoulos, Real gas normal shock waves with the Redlich-Kwong equation of state, Acta Mech. **76**, 223 (1989).

[6] R. Arina, Numerical simulation of near-critical fluids, Appl. Numer. Math. **51**, 409 (2004).

[7] E. Jassim, M. Abedinzadegan Abdi, and Y. Muzychka, Computational fluid dynamics study for flow of natural gas through high-pressure supersonic nozzles: Part 1. Real gas effects and shockwave, Pet. Sci. Technol. **26**, 1757 (2008).

[8] W. A. Sirignano, Compressible flow at high upstream pressure with linear equation of state, J. Fluid Mech. **843**, 244 (2018).

[9] A. Kluwick, Transonic nozzle flow of dense gases, J. Fluid Mech. **247**, 661 (1993).

[10] B. E. Poling, J. M. Prausnitz, and J. P. O'Connell, *The Properties of Gases and Liquids*, 5th ed. (McGraw Hill, New York, 2001).

[11] H. W. Liepmann and A. Roshko, *Elements of Gasdynamics* (Wiley, London, 1957).

[12] J. Lighthill, *Waves in Fluids* (Cambridge University Press, Cambridge, 1978).

[13] D. M. Dattelbaum, P. M. Goodwin, D. B. Garcia, R. L. Gustavsen, J. M. Lang, T. D. Aslam, S. A. Sheffield, L. L. Gibson, and J. S. Morris, Shockwave compression of Ar gas at several initial densities, *Shock Compression of Condensed Matter - 2015: Proceedings of the Conference of the American Physical Society Topical Group on Shock Compression of Condensed Matter*, AIP Conf. Proc. 1793 (AIP, New York, 2017), p. 090004.